

Article

Formation of the Liaotianshan Volcano in Southeastern China: Implications for the Evolution and Recharge of Crustal Magma System

Boyun Shi ¹, Lei Liu ^{1,2,3,*} and Zengxia Zhao ^{1,2,3,*}

¹ Guangxi Key Laboratory of Hidden Metallic Ore Deposits Exploration, College of Earth Sciences, Guilin University of Technology, Guilin 541006, China; m18810879972@163.com

² Collaborative Innovation Center for Exploration of Nonferrous Metal Deposits and Efficient Utilization of Resources, Guilin University of Technology, Guilin 541006, China

³ Guangxi Science Innovation Base for Formation and Exploration of Strategic Critical Mineral Resources, Guilin University of Technology, Guilin 541006, China

* Correspondence: liulei@glut.edu.cn (L.L.); zhaozx@glut.edu.cn (Z.Z.)

Abstract: Large-volume volcanic activity may offer significant insights into the evolution of silicic magma systems. The Liaotianshan volcano represents one of the earliest and best-preserved examples in SE China, comprising two stages of silicic volcanic rocks followed by extrusive rhyolite porphyries within the conduit. In this study, we present petrological and geochemical analyses, along with zircon dating, of the Liaotianshan volcano. LA-ICP-MS zircon U-Pb dating results revealed that two-stage eruptions occurred between approximately 160 and 157 Ma, and the latest batch of magma was extruded from the conduit around 153 Ma. Volcanic rocks from both stages exhibit similar geochemical compositions, characterized by pronounced depletion in high-field-strength elements and enrichment in large-ion lithophile elements, with the majority of zircon $\varepsilon_{\text{Hf}}(t)$ values falling within a narrow range of -9.8 to -5.4 . In contrast, the extrusive rhyolite porphyries display distinct geochemical characteristics, demonstrating enrichment in heavy rare earth elements relative to light rare earth elements [$(\text{La}/\text{Yb})_{\text{N}} = 0.14\text{--}0.61$], obvious negative Eu anomalies ($\text{Eu}/\text{Eu}^* = 0.01\text{--}0.03$), and positive Ce anomalies, alongside markedly depleted zircon Hf isotopic compositions. We propose that the volcanic rocks from the two stages were formed by the reworking of the Paleoproterozoic crustal basement with occasional recharge of parental magma, while the extrusive rhyolite porphyries resulted from the mixing of crustal-derived magma and significantly depleted mantle-derived materials. The Liaotianshan volcano was formed in contradiction to the model of melt extraction and crystal accumulation within a magma chamber, instead reflecting the evolutionary history and replenishment dynamics of the crustal magma system.

Keywords: volcanic activity process; magma system evolution; magma recharge; Late Mesozoic; Liaotianshan volcano; SE China



Citation: Shi, B.; Liu, L.; Zhao, Z. Formation of the Liaotianshan Volcano in Southeastern China: Implications for the Evolution and Recharge of Crustal Magma System. *Minerals* **2024**, *14*, 1263. <https://doi.org/10.3390/min14121263>

Academic Editors: Petrus J Le Roux, Benigno E. Godoy, Inés Rodríguez and Marco Taussi

Received: 16 November 2024

Revised: 7 December 2024

Accepted: 11 December 2024

Published: 12 December 2024



Copyright: © 2024 by the authors. Licensee MDPI, Basel, Switzerland. This article is an open access article distributed under the terms and conditions of the Creative Commons Attribution (CC BY) license (<https://creativecommons.org/licenses/by/4.0/>).

1. Introduction

The emplacement and eruption mechanisms of large-volume silica-rich magmas are of crucial significance for comprehending the differentiation and evolution of the continental crust [1–3]. However, the origin of the volcanic rocks and their association with plutonic rocks remain highly controversial. Some scholars propose a close relationship between volcanic and plutonic rocks, suggesting that rhyolitic melts could accumulate at the top of a magma reservoir and subsequently erupt, leaving the plutonic rocks as remnant cumulates [4,5]. In contrast, others contend that rapid eruptions of silicic magmas occur at high magma flux, leaving behind only minor plutonic residues [6], while significant plutonic assembly is generated at low magma flux [7,8]. Nevertheless, it is widely agreed that shallow plutons in large silicic calderas have a close genetic connection with the coexisting

volcanic rocks [4,7,9]. The eruptions commonly partially evacuate the magma chamber, leaving behind its remnants as associated shallow plutons and sometimes extrusions in the volcanic conduit [4]. Therefore, the origin of large-volume volcanism is of paramount importance for the comprehension of the nature and evolution of the mid- to upper crustal magma system, as it records the complex history of magma accumulation, fractionation, mixing, and replenishment [4,7,8].

Late Mesozoic silicic magmatism is intensive along the coastal area of SE China, forming a large-scale volcanic–plutonic complex belt [10,11] (Figure 1). Numerous studies on the Cretaceous volcanic–plutonic complexes have been conducted, suggesting that the volcanic rocks and subvolcanic plutons within a volcano were co-magmatic [9,12,13]. However, detailed evaluation of the relationship between Jurassic volcanic and shallow plutonic rocks has received only minimal attention. Here, we present a case study on the Liaotianshan volcano, one of the earliest and best-preserved Late Mesozoic volcanos in SE China [14], to constrain the crystallization ages, the nature of the magma sources, and magmatic differentiation, which would assist in assessing the genetic relationship between the volcanic and plutonic rocks.

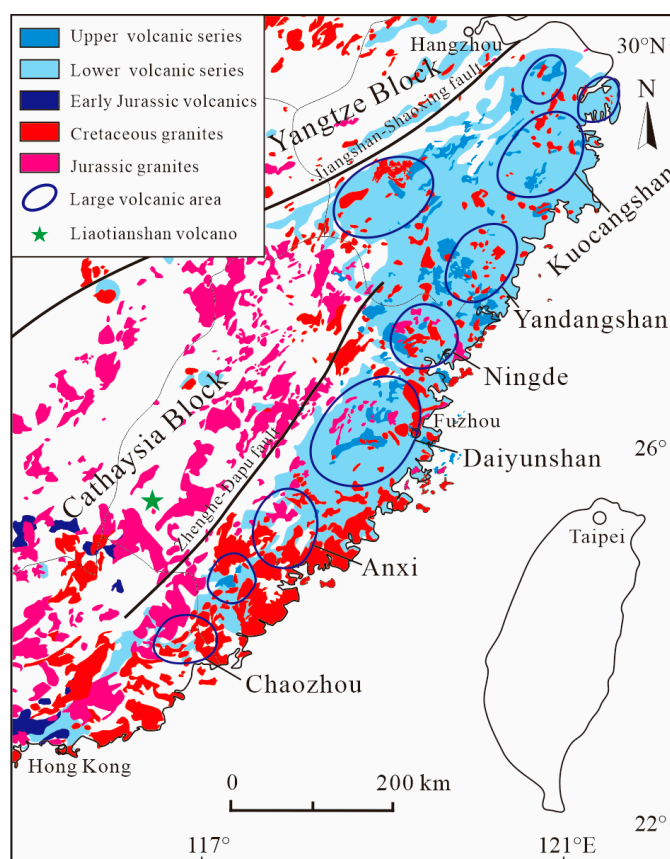


Figure 1. Distribution of Late Mesozoic volcanic–intrusive rocks in SE China (modified after [10]).

2. Geological Background

The South China Block is composed of two major Precambrian continental blocks: the Yangtze Block in the northwest and the Cathaysia Block in the southeast. These blocks were merged during the Neoproterozoic along the Jiangshan–Shaoxing fault [15] (Figure 1). In the eastern Cathaysia Block, Paleoproterozoic to Neoproterozoic granites and high-grade metamorphic rocks are extensively distributed, and they are intruded by Early Paleozoic and Late Mesozoic granites or overlain by Paleozoic sediments and Late Mesozoic silicic volcanic rocks [11,16]. The Late Mesozoic volcanic rocks mainly comprise rhyolitic pyroclastic rocks and rhyolite lavas. They outcrop in several large volcanic fields that contain calderas or volcano complexes closely associated with shallow intra-caldera

plutons, covering a total outcrop area of about 90,000 km² [9–11,17] (Figure 1). Traditionally, these volcanic rocks were classified into lower and upper series, which were emplaced during ca. 160–120 Ma and 110–85 Ma, respectively [11].

The Liaotianshan volcano, located in southwestern Fujian Province, shows an irregular semi-elliptical shape with an outcrop area of about 23 km², unconformably overlying the lower Carboniferous and lower–middle Permian strata, as well as early Jurassic biotite syenogranite (Figure 2a). The center of the volcano is situated within the steep and elevated Liaotianshan–Nanshanding area. The complete volcanic eruption process can be broadly divided into two stages based on the lithology and lithofacies association. The products of the first eruption stage primarily consist of tuffaceous sandstones and mudstones associated with eruption–sedimentary facies, along with rhyolitic/dacitic crystal-lithic tuffs in air-fall facies; these are sporadically distributed around the periphery of the volcanic basin. The second eruption stage was marked by more intense volcanic activity that generated rhyodacites and rhyolitic crystal-lithic tuffs, breccia-bearing rhyolitic tuffs, and ignimbrites interbedded with tuffaceous sandstones and mudstones. The products of this second eruption stage constitute the main body of the volcano. The volcanic conduit is positioned at Liaotianshan and is filled with rhyolite porphyries exhibiting extrusion facies. Various lithologies and facies are arranged in semi-concentric patterns, forming an overall inward-dipping ring structure with dip angles ranging from 11° to 35° (Figure 2b).

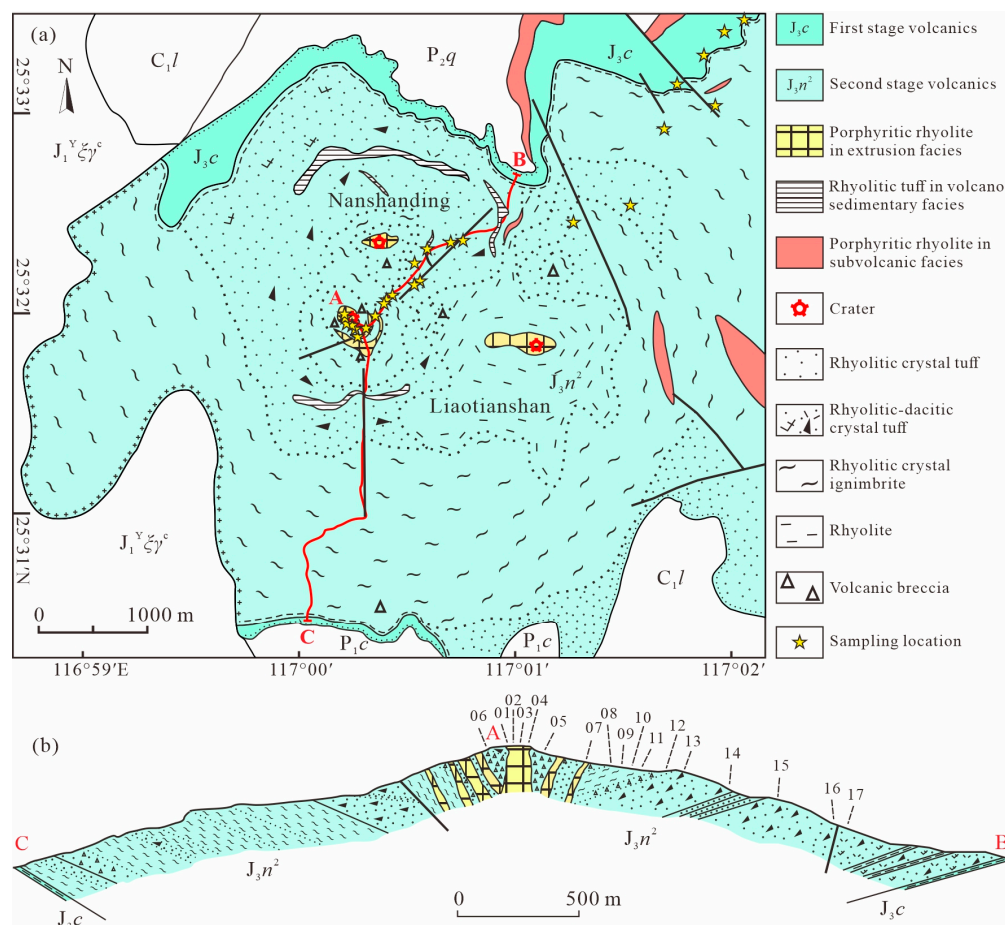


Figure 2. (a) Geological map of the Liaotianshan volcano and sample locations (modified after [14]); (b) profile of the section from which the samples were collected. Notes: $J_1^Y \xi \gamma^C$ —early Jurassic biotite syenogranite; C_1l —lower Carboniferous Lindi Formation; P_1c —lower Permian Chuanshan Formation; P_2q —middle Permian Qixia Formation. The letters A, B, and C represent the end positions of the section profile in both (a,b).

3. Samples and Methods

The samples analyzed in this study were collected from the northeastern flank of the Liaotianshan volcano. The collection includes four rhyolitic crystal-lithic welded tuffs from the first eruption stage, sixteen volcanic rocks from the second eruption stage, and five rhyolite porphyries from the volcanic conduit (Figure 2; Table S1). The rhyolite porphyries are flesh-red in color and possess a porphyritic texture. Phenocrysts constitute 10%–15% of the rock, with grain sizes ranging from 0.5 to 4.5 mm. These phenocrysts are primarily composed of quartz, plagioclase, and alkali feldspar, while the matrix displays a microgranular texture consisting of fine quartz (Figure 3a,b). The second-stage breccia-bearing rhyolitic welded tuffs, situated near the conduit, are characterized by gray or purple hues and comprise fine lithic fragments alongside crystal fragments and other components. These rocks contain 3%–5% lithics, with sizes reaching up to centimeters. These breccias are irregularly shaped and randomly distributed, comprising materials such as rhyolite and tuff (Figure 3c,d). In contrast, the first-stage crystal-rich welded tuffs, located further away from the conduit, show little to no presence of lithics; they predominantly consist of crystal fragments including alkali feldspar, plagioclase, and quartz, typically not exceeding a content level of 20%. Notably, at the base of these first-stage-welded tuffs is an increased concentration of ductile pumice fragments (Figure 3e,f).

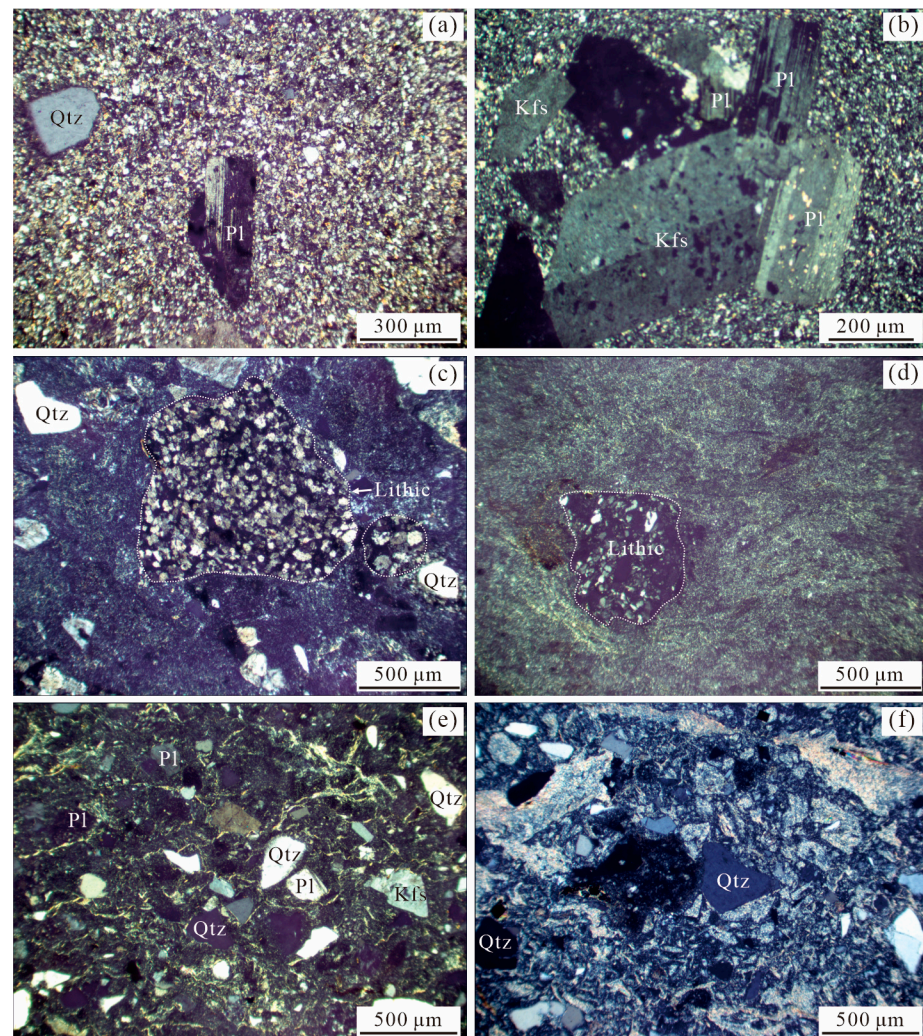


Figure 3. Representative photomicrographs of (a,b) the rhyolite porphyries from the volcanic conduit, (c,d) the second-stage lithic-bearing volcanic rocks, and (e,f) the first-stage crystal-rich volcanic rocks, respectively. Notes: Pl—plagioclase; Kfs—K-feldspar; Qtz—quartz.

All analyses were carried out at the Guangxi Key Laboratory of Hidden Metallic Ore Deposits Exploration, Guilin University of Technology, China.

Zircon cathodoluminescence (CL) images were obtained to characterize the internal structures. Zircon U–Pb dating was performed using an Agilent 7500 inductively coupled plasma–mass spectrometry (ICP–MS) instrument equipped with a GeoLas HD laser sampler. Zircon trace element analyses were performed concurrently with the U–Pb isotopic dating analyses. All analyses employed a beam diameter of 32 μm , a repetition rate of 6 Hz, and a laser energy of 10 J/cm². The specific instrumental settings and analytical procedures adhered to those outlined by [18]. The Lu–Hf isotopic composition measurements involved analysis within similar domains of the zircon crystal used for U–Pb dating as determined from CL images. In situ zircon Hf isotope analyses were conducted using a GeoLas HD laser ablation system in conjunction with a Neptune Plus multi-collector–ICP–MS instrument. The specific instrumental settings and analytical procedures are the same as [14].

Whole-rock major element analyses were conducted using X-ray fluorescence techniques. Loss-on-ignition (LOI) values for each sample were determined after heating to 1000 °C. Trace element analyses were performed with an Agilent 7900CX ICP–MS instrument following the acid dissolution of the samples. The analytical precision was better than $\pm 5\%$ for major elements and ranged from $\pm 2\%$ to $\pm 5\%$ for most trace elements.

4. Results

4.1. Zircon U–Pb Geochronology

The zircon crystals from different samples display consistent features, shown as euhedral to subhedral elongated prisms with lengths ranging from 100 to 200 μm . The CL images of zircons separated from the first- and second-stage volcanic rocks show well-developed oscillatory zoning, with certain zircons exhibiting narrow dark bands that indicate fluctuations in the zircon crystallization rate and magma replenishment processes [19] (Figure 4). In contrast, the CL images of zircon from extrusive rhyolite porphyry are significantly darker, with only a limited number of grains displaying faint oscillatory zoning. Additionally, some grains show internal structural damage associated with elevated concentrations of radioactive elements thorium and uranium within the zircon (Figure 4).

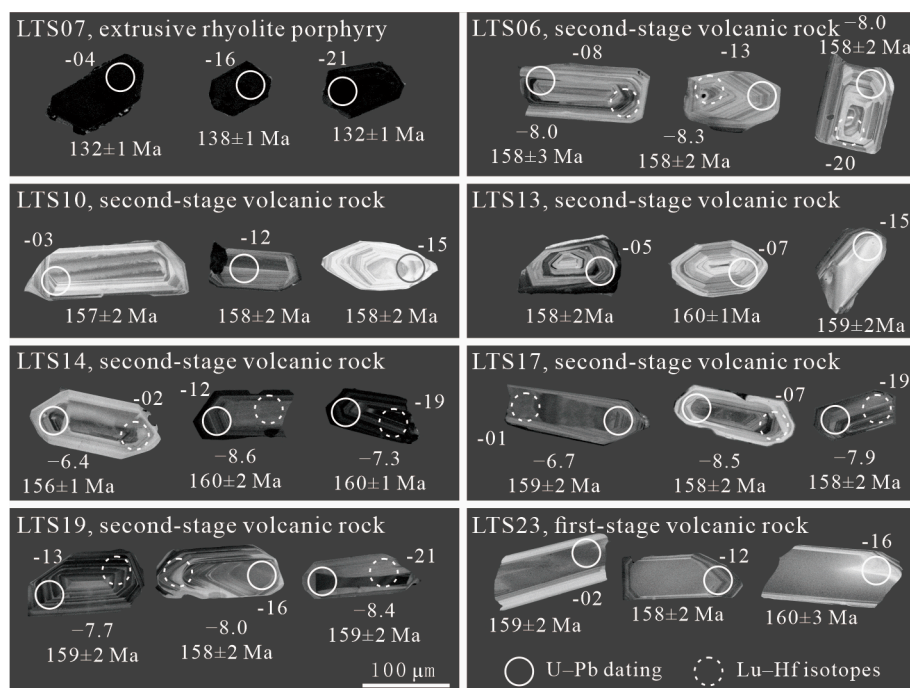


Figure 4. Cathodoluminescence images of representative zircons from the Liaotianshan volcano.

The results of LA-ICP-MS zircon U–Pb dating indicate that most analyses of the first- and second-stage volcanic rocks are concordant or nearly concordant (Figure 5; Table S2). One sample from the first-stage volcanic products yields a weighted mean $^{206}\text{Pb}/^{238}\text{U}$ age of 159.9 ± 0.9 Ma, while six samples from different layers of the second-stage volcanic successions yield similar ages ranging from 157.2 ± 1.0 to 158.8 ± 1.0 Ma. However, the dating results of the extrusive rhyolite porphyry yield few concordant ages (Figure 5a); even the limited number of concordant ages are significantly younger than previously reported values (153.2 ± 0.7 Ma [14]). Additionally, the first-stage volcanic rocks contain several inherited zircons from the Neoproterozoic (1046–945 Ma), Paleozoic (402 Ma), and Middle Triassic (246–243 Ma) periods, whereas the second-stage volcanic rocks include a limited number of captured zircons from the Paleozoic (420–369 Ma).

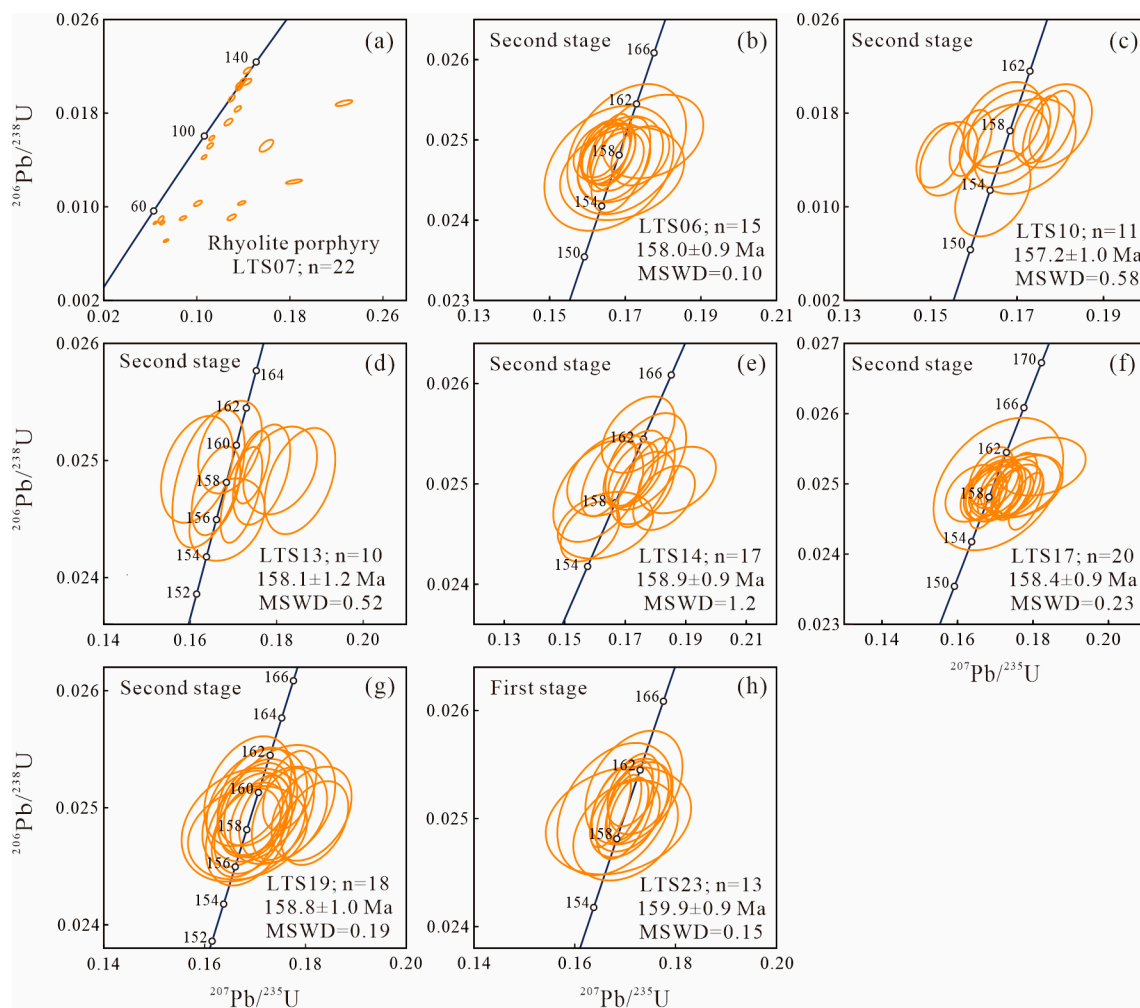


Figure 5. Zircon U–Pb dating results for (a) extrusive rhyolite porphyry, (b–g) second-stage volcanic rocks, and (h) first-stage volcanic rock, respectively.

4.2. Zircon Trace Elements

The trace elements of zircons in the analyzed first- and second-stage volcanic rock samples largely overlap with each other (Figure 6; Table S3). These zircons exhibit significantly depleted concentrations of light rare earth elements (REEs) but enriched concentrations of heavy REEs, accompanied by pronounced negative Eu anomalies ($\text{Eu}/\text{Eu}^* \leq 0.62$, and 84% of them ≤ 0.40) and positive Ce anomalies ($\text{Ce}/\text{Ce}^* \geq 1.48$). With the exception of a few grains exhibiting slightly enriched La contents (> 1 ppm), potentially due to micro-inclusions and therefore excluded from subsequent statistical analysis [20], the remaining zircons display consistent Th (45.0–1901 ppm), U (76.5–2673 ppm), and Ti (1.32–11.3 ppm)

concentrations, while demonstrating enriched Hf (7883–13740 ppm) and Y (424–3549 ppm) contents. The trace elements of zircons in the extrusive rhyolite porphyry, on the contrary, exhibit distinct features characterized by conspicuous enrichment of light REEs. Meanwhile, the concentrations of heavy REEs exhibit an order of magnitude higher than those observed in the zircons from both the first- and second-stage volcanic rocks.

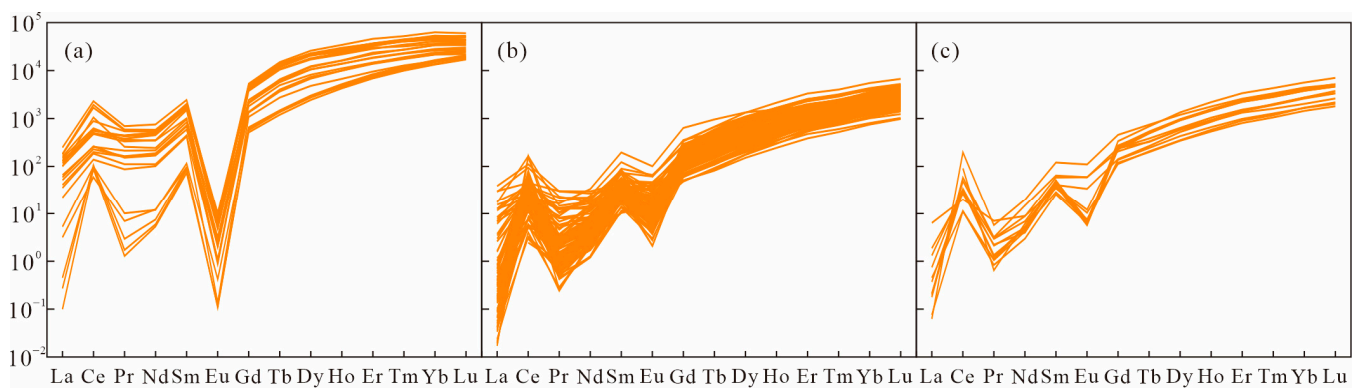


Figure 6. Chondrite-normalized REE patterns for the zircons from (a) extrusive rhyolite porphyry, (b) second-stage volcanic rocks, and (c) first-stage volcanic rock, respectively (normalization values after [21]). Patterns of the inherited grains are not presented.

4.3. Zircon Hf Isotopes

The zircon Lu–Hf isotopic composition of four samples from the second-stage volcanic rocks was analyzed, which exhibit a generally homogeneous distribution, displaying a symmetrical bell-shaped pattern. Apart from four analyses exhibiting $\epsilon_{\text{Hf}}(t)$ values ranging from -13.6 to -10.3 , the remaining grains display $\epsilon_{\text{Hf}}(t)$ values within a narrow range of -9.8 to -5.4 (Figure 7; Table S4). Excluding the outliers, the weighted mean $\epsilon_{\text{Hf}}(t)$ values for the analyzed second-stage volcanic rock samples are -8.3 ± 0.4 , -7.8 ± 0.4 , -7.7 ± 0.4 , and -8.2 ± 0.4 , respectively. These values align with those of the first-stage volcanic rocks (-8.0 ± 0.3) but exhibit a lower magnitude compared to that of the extrusive rhyolite porphyry (-3.9 ± 0.4) [14]. Moreover, the zircon $\epsilon_{\text{Hf}}(t)$ values correspond to two-stage model ages (T_{DM2}) of 1.80–1.52 Ga for the majority and 2.04–1.83 Ga for the outliers.

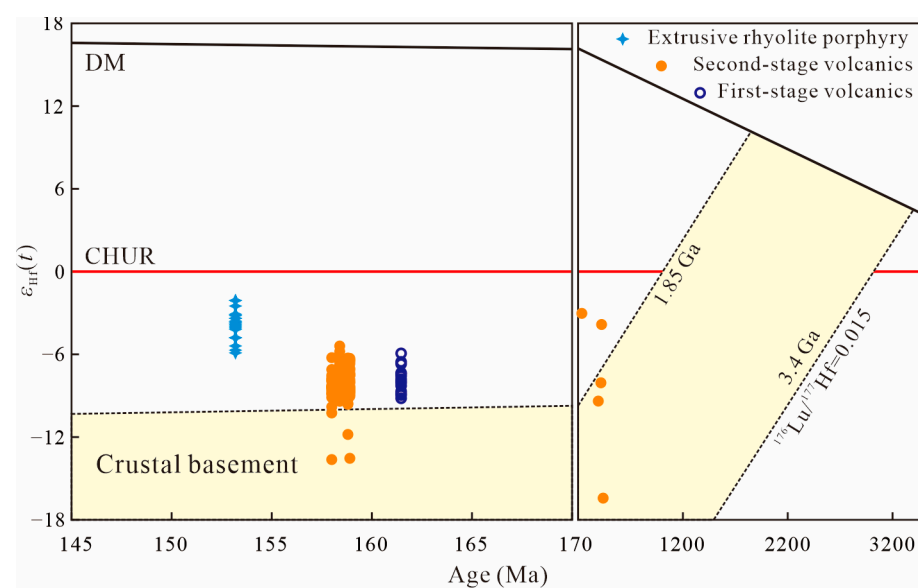


Figure 7. Zircon Hf isotopic compositions of the Liaotianshan volcano and crustal basement materials [22]. The values of the extrusive rhyolite porphyry and first-stage volcanics are from [14].

4.4. Whole-Rock Major and Trace Elements

The first- and second-stage volcanic rocks exhibit similar major elemental compositions, with combined SiO_2 contents varying widely from 71.69 wt% to 82.42 wt% and total alkali ($\text{K}_2\text{O} + \text{Na}_2\text{O}$) contents of 2.99–9.46 wt%, thus classifying them as rhyolites (Figure 8; Table S5). Conversely, the extrusive rhyolite porphyries possess a narrow major elemental composition range, with SiO_2 contents spanning from 75.31 wt% to 76.16 wt%. Furthermore, all the analyzed samples demonstrate enriched Al_2O_3 contents (>10.37%), while presenting depleted TiO_2 (<0.34 wt%), total Fe_2O_3 ($\text{Fe}_2\text{O}_3^{\text{T}}$, <2.30 wt%), MnO (<0.07 wt%), MgO (<0.44 wt%), and P_2O_5 (<0.04 wt%) contents. Overall, the above major-element oxides decrease linearly as SiO_2 increases (Figure 8).

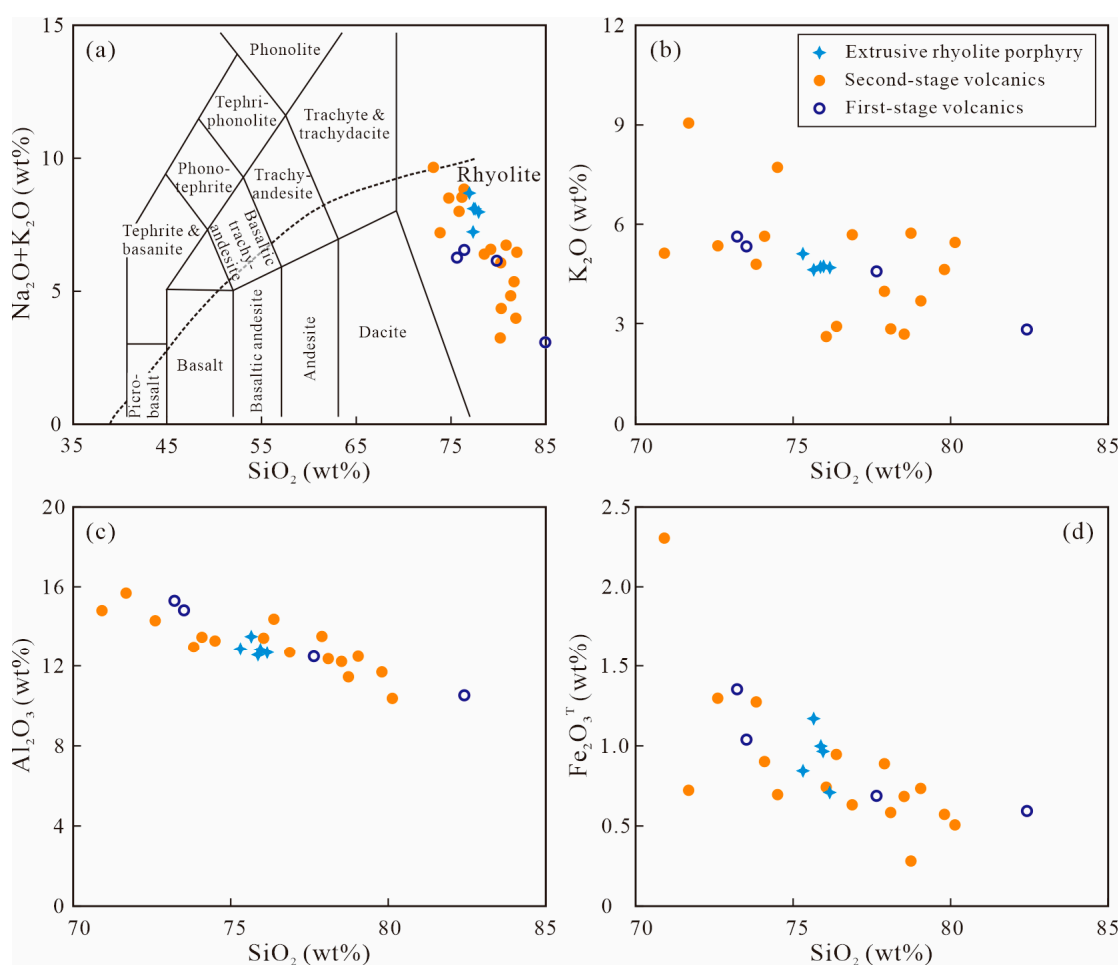


Figure 8. (a) Total alkali [23], (b) K_2O , (c) Al_2O_3 , and (d) $\text{Fe}_2\text{O}_3^{\text{T}}$ vs. SiO_2 diagrams for rocks of the Liaotianshan volcano.

The first- and second-stage volcanic rocks demonstrate similar trace elemental compositions as well, featuring pronounced depletion in high-field-strength elements (HFSEs), such as Nb, Ta, Ti, and P, and enrichment in large-ion lithophile elements (LILEs), such as Rb and K (Figure 9). The volcanic rocks also present fractionation characterized by enrichment in light REEs [(La/Yb)_N = 2.21–33.90], with moderately negative Eu anomalies ($\text{Eu}/\text{Eu}^* = 0.07\text{--}0.50$) and slightly negative Ce anomalies ($\text{Ce}/\text{Ce}^* = 0.60\text{--}0.96$ for most of the samples). In contrast, the extrusive rhyolite porphyries display distinct trace elemental characteristics, showing enrichment in heavy REEs [(La/Yb)_N = 0.14–0.61], with obvious negative Eu anomalies ($\text{Eu}/\text{Eu}^* = 0.01\text{--}0.03$) and positive Ce anomalies ($\text{Ce}/\text{Ce}^* = 1.00\text{--}3.85$).

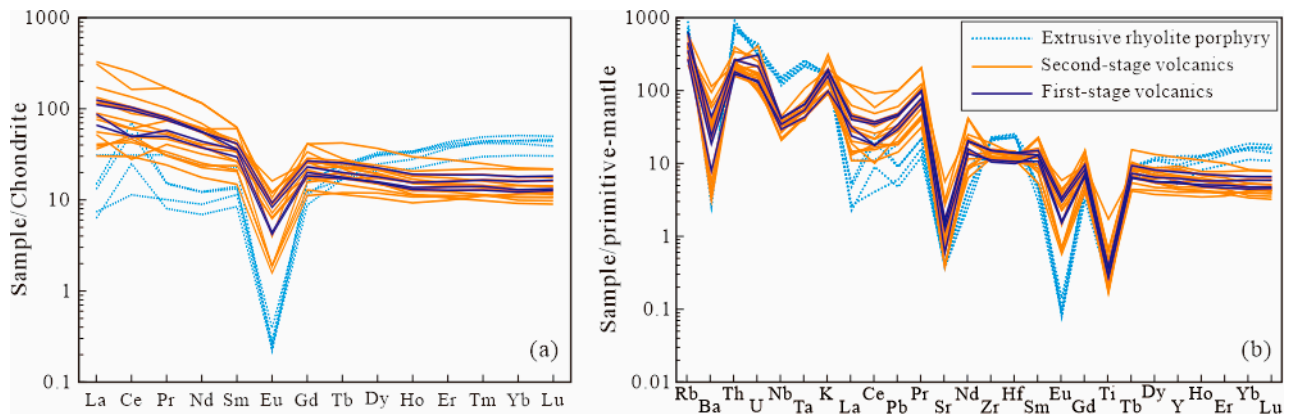


Figure 9. (a) Chondrite-normalized REE patterns [21], and (b) primitive-mantle-normalized trace element variation diagram [24] for rocks of the Liaotianshan volcano.

5. Discussion

5.1. Affinities of the Zircons and Their Constraints on the Timescale of the Volcanic Activity

Mounting evidence suggests that many large intrusions do not stem from a single magma emplacement followed by crystallization; instead, they originate from the cumulative emplacement of pulsating magmas over timescales ranging from thousands to millions of years [25,26]. Likewise, large-volume volcanic eruptions can also endure for the same or even a longer time scale [9]. A potential ≤ 100 ky overestimation of zircon-based eruption ages compared to $^{40}\text{Ar}/^{39}\text{Ar}$ -based deposition ages for volcanic tephra has been proposed [27]. This pre-eruption time of zircon crystals is negligible in comparison with the analytical uncertainties. Therefore, the zircon U–Pb dating results are regarded as the eruption and deposition ages of the studied Liaotianshan volcanic successions.

As noted previously, zircons in the first- and second-stage volcanic rocks display comparable morphology, internal structure, and trace elemental compositions (Figure 6). Moreover, these zircons show a linearly decreasing trend in Ti contents and Th/U and Eu/Eu* values as Hf contents increase (Figure 10), demonstrating them to be magmatic zircons, which crystallized within a stable magmatic evolution system [28]. On the contrary, zircons in the extrusive rhyolite porphyry display entirely different internal structure and trace elemental characteristics (Figure 6). Additionally, they possess distinct Th and Ti contents, as well as $(\text{Sm}/\text{La})_{\text{N}}$ and Eu/Eu* values, which are different from those of the grains in the first- and second-stage volcanic rocks (Figure 10). Their low $(\text{Sm}/\text{La})_{\text{N}}$ and Ce anomalies further suggest a late-stage hydrothermal origin [28]. From this perspective, the latest-stage extrusive rhyolite porphyries in the Liaotianshan volcano crystallized in a fundamentally different magma from the previous volcanic rocks.

The differences in the zircon trace elemental patterns lead to another consequence that the dating analyses for the extrusive rhyolite porphyry fail to yield reasonable results (Figure 5). Fortunately, Liu et al. [14] presented a qualified age of 153.2 ± 0.7 Ma for the rhyolite porphyry, which is approximately 4 Ma younger than the adjoining second-stage volcanic rocks. The time hiatus is sufficiently long for significant changes to occur in the magmatic system. On the other hand, the first- and second-stage volcanic rocks have indistinguishable ages (159.9 ± 0.9 to 157.2 ± 1.0 Ma), hence suggesting that they were derived from a successive magmatic cycle. In conclusion, the large-volume eruption primarily took place between approximately 160 and 157 Ma in the study area, possibly occurring in several rounds due to interbedded sediments. Subsequently, the most recent batch of magma was extruded from the conduit around 153 Ma; however, its composition has undergone notable changes.

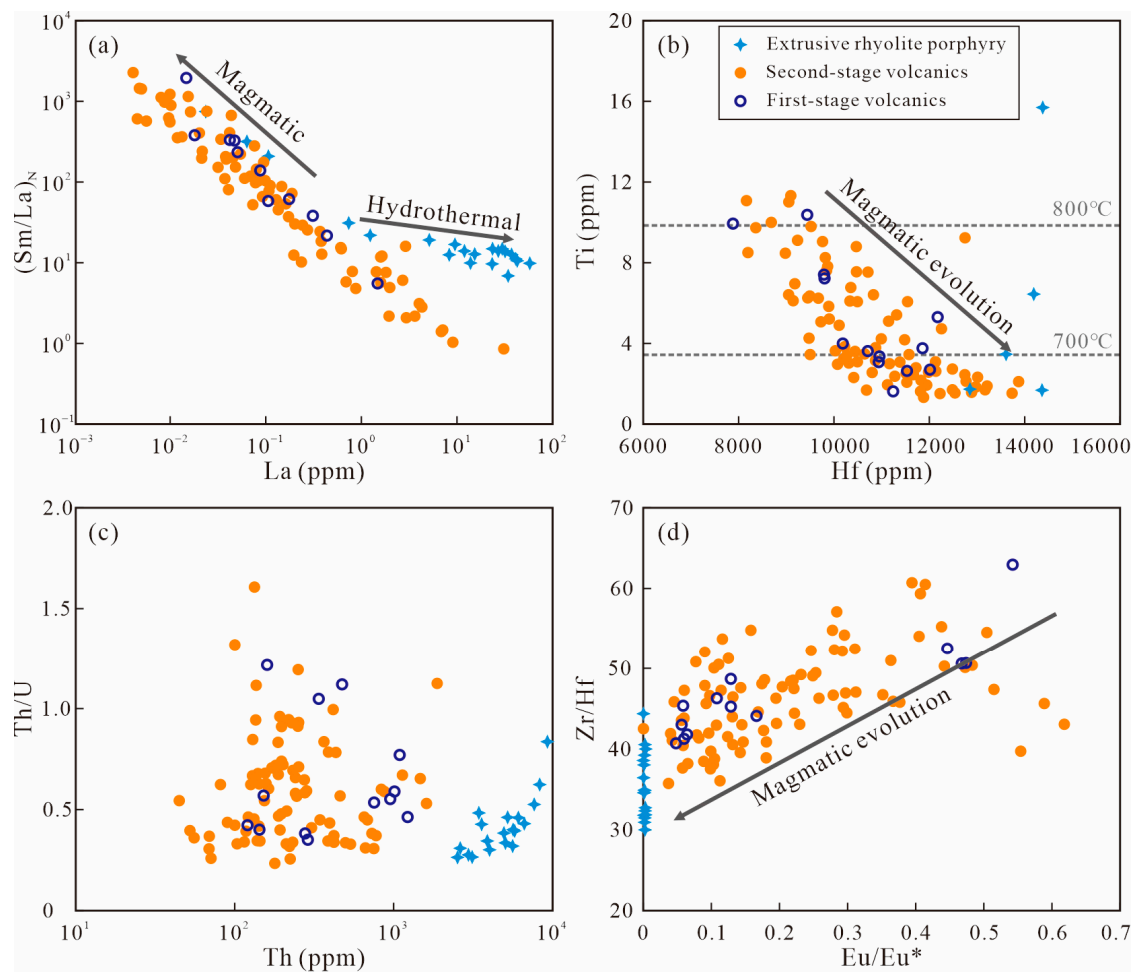


Figure 10. (a) $(\text{Sm}/\text{La})_N$ vs. La, (b) Ti vs. Hf, (c) Th/U vs. Th and (d) Zr/Hf vs. Eu/Eu* variations in zircons of the Liaotianshan volcano.

5.2. Evolution and Replenishment of the Magma

Apart from the indistinguishable eruption and deposition ages, the first- and second-stage volcanic rocks have highly similar zircon Lu–Hf isotopic compositions (Figure 7). Consequently, both stages of volcanic rocks could have originated from a common magma source. It is widely acknowledged that the continental crust constitutes a significant contributor to the voluminous silicic magmas [29]. The enriched zircon Lu–Hf isotopic compositions indicate that the Liaotianshan volcanic rocks originated predominantly from the partial melting of the Paleoproterozoic crustal basement. Moreover, the narrow range of zircon $\varepsilon_{\text{Hf}}(t)$ values, in conjunction with low magma temperatures ($<829^\circ\text{C}$) determined using a Ti-in-zircon thermometer, implies the scarce involvement of juvenile materials. With that being said, crustal contamination might play a limited role in the volcanic activity, owing to the small number of inherited zircons present in the volcanic products.

As shown in Harker diagrams (Figure 8), the first- and second-stage volcanic rocks exhibit a linear tendency of selected major-element oxides that correlate well with SiO_2 contents. A favorable linear correlation among trace elements was also observed among these volcanic rocks (Figure 11). All these volcanic samples present negative Ba, Eu, Sr, and Ti anomalies, as well as distinct positive Rb anomalies, in their normalized trace element patterns (Figure 9), indicating the removal of alkali feldspar and plagioclase during magma differentiation [30].

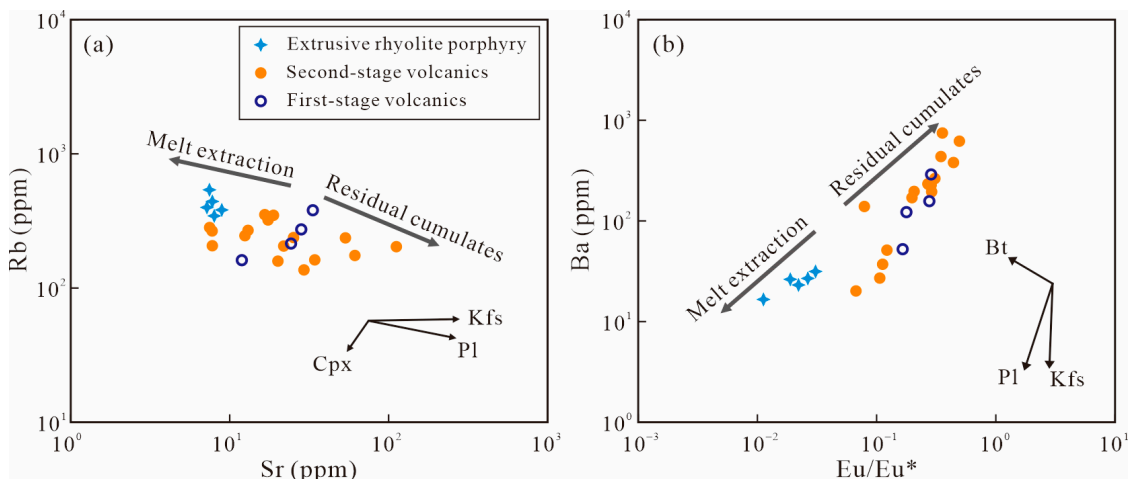


Figure 11. (a) Rb vs. Sr and (b) Ba vs. Eu/Eu* variations of extrusive and volcanic rocks from the Liaotianshan volcano, which are inconsistent with the melt extraction and residual cumulates model.

It has been shown that, in some cases, the earliest volcanic products within a silica-rich volcano have the lowest SiO₂ content, demonstrating the least-evolved features [9]. The subsequent volcanic units are likely the result of crystal fractionation from a parental magma close to that of the earliest volcanic products, such as in the Cretaceous Yandangshan caldera, SE China [9]. However, the first-stage volcanic rocks in the Liaotianshan volcano yield similar ranges of content for SiO₂ and other major-element oxides (Figure 8), as well as (La/Yb)_N and Eu/Eu* values (Figure 9), when compared to the second-stage volcanic rocks. In addition, the SiO₂ contents of the volcanic rocks from the early to late parts of the volcano fluctuate on multiple occasions (Figure 12). This may indicate that corresponding magma recharge events took place during the prolonged volcanic activity [31]. The injection of parental magma led to the magma reservoir being chemically less evolved. The recharge of the magma chamber by the arrival of a new magma batch is almost ubiquitous at an active volcano [32,33].

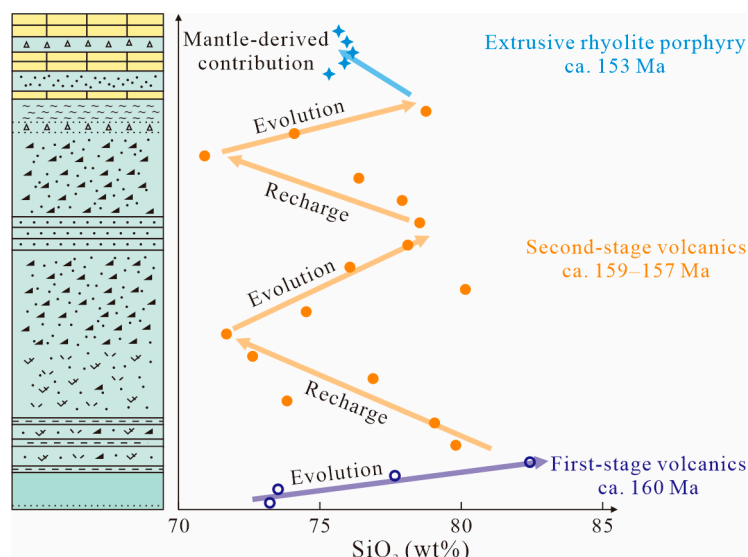


Figure 12. Fluctuation in the SiO₂ contents of the volcanic rocks from the early to late parts of the volcano.

5.3. Petrogenesis of the Extrusive Rhyolite Porphyries

The latest product within a volcano is typically composed of shallow plutons or subvolcanic porphyries associated with the previously formed volcanic rocks [4,7,9,17]. In

this case, the latest volcanic product likely formed by crystal accumulation in the magma chamber, resulting from the extraction and eruption of rhyolitic melts [30,34,35]. Thus, these rocks usually display geochemical characteristics that plot in a direction opposite to the fractional crystallization vectors defined by the previously formed volcanic rocks [5,7,9]. However, extrusive rhyolite porphyries in the Liaotianshan volcano do not exhibit the least-evolved geochemical characteristics. Their contents of SiO₂ and other major-element oxides are positioned in the middle of the ranges observed for first- and second-stage volcanic rocks (Figure 8). Moreover, the modeling of trace elements reveals a well-evolved trend that aligns with the associated volcanic rocks, which is inconsistent with the melt extraction and residual cumulates model (Figure 11). Therefore, the extrusive rhyolite porphyries within the Liaotianshan volcano are inferred to have originated from a magma distinct from that which produced the first- and second-stage volcanic rocks, as also indicated by the zircon trace element patterns.

The extrusive rhyolite porphyries display significantly depleted zircon Hf isotopic compositions in comparison to the first- and second-stage volcanic rocks (Figure 7), implying an alternative petrogenesis involving partial melting of different resources or mixing between ancient- and mantle-derived magmas. In fact, Late Mesozoic volcanic–plutonic rocks in SE China exhibit a universal trend of increasing radiogenetic zircon Hf isotopic compositions over time [13,14,36,37]. This phenomenon has been extensively discussed and widely accepted as resulting from an increasing contribution of mantle-derived materials, plausibly driven by enhanced lithospheric extension associated with paleo-Pacific subduction [13]. We advocate for the magma mixing model to explain the generation of the extrusive rhyolite porphyries, not only because it accounts for their less-evolved characteristics, such as depletion in incompatible elements, but also due to its alignment with the storage configuration of the magma reservoir within the crust (see below).

Recent models regarding the formation, storage, and chemical differentiation of magma within the Earth's crust have been emphasized to encompass the entire crust, i.e., the trans-crustal magmatic systems [3,38]. A deep crustal hot zone could be generated by mantle-derived basaltic magma injecting into the lower crust, which generates and promotes the partial melting of pre-existing crustal rocks [39]. The crust-derived melts ascend from the hot zone to form a deep acidic magma reservoir in the mid- to upper crust, feeding and recharging a shallow upper crustal magma chamber, which is necessary for the generation of high-silica rhyolitic rocks [40]. The prolonged volcanic activity of the Liaotianshan volcano, along with occasional injections of parental magma, further corroborates the existence of both a shallow magma chamber and a deep magma reservoir. Developed in contradiction to the melt extraction and crystal accumulation model, the volcanic and extrusive rocks within the Liaotianshan volcano exemplify a scenario that reflects the evolutionary history and replenishment dynamics of the crustal magma system.

6. Conclusions

The first- and second-stage volcanic rocks within the Liaotianshan volcano were formed continuously during 160–157 Ma, and the latest rhyolite porphyries extruded around 153 Ma. These volcanic rocks originated from partial melting of Paleoproterozoic crustal basement, with occasional injections of parental magma resulting in a less chemically evolved magma reservoir during its evolution. In contrast, the geochemical differences observed in the extrusive rhyolite porphyries are primarily attributed to contributions of mantle-derived materials into the ancient crust-derived magmas. The Liaotianshan volcano developed in contradiction to the model of melt extraction and crystal accumulation within a magma chamber, instead reflecting the evolutionary history and replenishment dynamics of the crustal magma system.

Supplementary Materials: The following supporting information can be downloaded at: <https://www.mdpi.com/article/10.3390/min14121263/s1>, Table S1: Lithologies, pyroclastic/mineral assemblages, and sample locations of the rocks from the Liaotianshan volcano; Table S2: LA-ICP-MS zircon U-Pb dating results of the rocks from the Liaotianshan volcano; Table S3: LA-ICP-MS zircon trace element

concentrations (ppm) of the rocks from the Liaotianshan volcano (the temperatures were estimated using Ti-in-zircon thermometry [41]); Table S4: Zircon Lu–Hf isotopic compositions of the rocks from the Liaotianshan volcano; Table S5: Whole-rock major (wt%) and trace element (ppm) contents of the rocks from the Liaotianshan volcano.

Author Contributions: Conceptualization, L.L. and Z.Z.; methodology, B.S.; formal analysis, B.S., L.L. and Z.Z.; investigation, B.S., L.L. and Z.Z.; data curation, B.S. and L.L.; writing—original draft preparation, B.S.; writing—review and editing, L.L. and Z.Z.; supervision, L.L.; project administration, L.L.; funding acquisition, L.L. and Z.Z. All authors have read and agreed to the published version of the manuscript.

Funding: This research was funded by the National Natural Science Foundation of China (42073031), Guangxi Science and Technology Program (Guike AD21220033), and the National Natural Science Foundation of China (42462003, 42263008).

Data Availability Statement: Data are contained within the article and Supplementary Materials.

Acknowledgments: We sincerely thank Zhenglin Li and Hongxia Yu for their technical support for sample analysis.

Conflicts of Interest: The authors declare no conflicts of interest.

References

1. Keller, C.B.; Schoene, B.; Barboni, M.; Samperton, K.M.; Husson, J.M. Volcanic–plutonic parity and the differentiation of the continental crust. *Nature* **2015**, *523*, 301–307. [[CrossRef](#)] [[PubMed](#)]
2. Lipman, P.W.; Bachmann, O. Ignimbrites to batholiths: Integrating perspectives from geological, geophysical, and geochronological data. *Geosphere* **2015**, *11*, 705–743. [[CrossRef](#)]
3. Cashman, K.V.; Sparks, R.S.J.; Blundy, J.D. Vertically extensive and unstable magmatic systems: A unified view of igneous processes. *Science* **2017**, *355*, eaag3055. [[CrossRef](#)] [[PubMed](#)]
4. Lipman, P.W. The roots of ash flow calderas in western North America: Windows into the tops of granitic batholiths. *J. Geophys. Res. Solid Earth* **1984**, *89*, 8801–8841. [[CrossRef](#)]
5. Bachmann, O.; Miller, C.F.; de Silva, S.L. The volcanic–plutonic connection as a stage for understanding crustal magmatism. *J. Volcanol. Geotherm. Res.* **2007**, *167*, 1–23. [[CrossRef](#)]
6. Jellinek, A.M.; DePaolo, D.J. A model for the origin of large silicic magma chambers: Precursors of caldera-forming eruptions. *Bull. Volcanol.* **2003**, *65*, 363–381. [[CrossRef](#)]
7. Glazner, A.F.; Bartley, J.M.; Coleman, D.S.; Gray, W.; Taylor, R.Z. Are plutons assembled over millions of years by amalgamation from small magma chambers? *GSA Today* **2004**, *14*, 4–12. [[CrossRef](#)]
8. Tappa, M.J.; Coleman, D.S.; Mills, R.D.; Samperton, K.M. The plutonic record of a silicic ignimbrite from the Latir volcanic field, New Mexico. *Geochem. Geophys. Geosyst.* **2011**, *12*, Q10011. [[CrossRef](#)]
9. Yan, L.-L.; He, Z.-Y.; Jahn, B.-M.; Zhao, Z.-D. Formation of the Yandangshan volcanic–plutonic complex (SE China) by melt extraction and crystal accumulation. *Lithos* **2016**, *266–267*, 287–308. [[CrossRef](#)]
10. Zhou, X.; Sun, T.; Shen, W.; Shu, L.; Niu, Y. Petrogenesis of Mesozoic granitoids and volcanic rocks in south China: A response to tectonic evolution. *Episodes* **2006**, *29*, 26–33. [[CrossRef](#)]
11. Liu, J.-X.; Wang, S.; Wang, X.-L.; Du, D.-H.; Xing, G.-F.; Fu, J.-M.; Chen, X.; Sun, Z.-M. Refining the spatio-temporal distributions of Mesozoic granitoids and volcanic rocks in SE China. *J. Asian Earth Sci.* **2020**, *201*, 104503. [[CrossRef](#)]
12. Du, D.H.; Wang, X.L.; Wang, S.; Miller, C.F.; Xu, X.S.; Chen, X.; Zhang, F.F. Deciphering Cryptic Multi-Stage Crystal-Melt Separation during Construction of the Tonglu Volcanic–Plutonic Complex, SE China. *J. Petrol.* **2022**, *63*, egab098. [[CrossRef](#)]
13. Xu, X.S.; Zhao, K.; He, Z.Y.; Liu, L. Cretaceous volcanic–plutonic magmatism in SE China and a genetic model. *Lithos* **2021**, *402–403*, 105728. [[CrossRef](#)]
14. Liu, L.; Zhao, Y.; He, Z.Y.; Sun, J.; Liu, X.J.; Zhao, Z.X. Activity process and petrogenesis of Liaotianshan caldera in SW Fujian: Evidence from zircon U–Pb, Hf isotopic and trace element concentrations. *Acta Geol. Sin.* **2023**, *97*, 2176–2194. (In Chinese with English abstract) [[CrossRef](#)]
15. Chen, J.F.; Jahn, B.M. Crustal evolution of southeastern China: Nd and Sr isotopic evidence. *Tectonophysics* **1998**, *284*, 101–133. [[CrossRef](#)]
16. Yu, J.-H.; O’Reilly, S.Y.; Griffin, W.L.; Zhou, M.-F.; Wang, L.-J. U–Pb geochronology and Hf–Nd isotopic geochemistry of the Badu Complex, Southeastern China: Implications for the Precambrian crustal evolution and paleogeography of the Cathaysia Block. *Precambrian Res.* **2012**, *222–223*, 424–449. [[CrossRef](#)]
17. Yan, L.-L.; He, Z.-Y.; Beier, C.; Klemd, R. Zircon trace element constrains on the link between volcanism and plutonism in SE China. *Lithos* **2018**, *320–321*, 28–34. [[CrossRef](#)]

18. Liu, Y.; Gao, S.; Hu, Z.; Gao, C.; Zong, K.; Wang, D. Continental and Oceanic Crust Recycling-induced Melt–Peridotite Interactions in the Trans-North China Orogen: U–Pb Dating, Hf Isotopes and Trace Elements in Zircons from Mantle Xenoliths. *J. Petrol.* **2010**, *51*, 537–571. [[CrossRef](#)]
19. He, Z.-Y.; Yan, L.-L. Zircon trace element geochemistry constrains on the silicic volcanic system. *Acta Petrol. Mineral.* **2021**, *40*, 939–951. (In Chinese with English abstract)
20. Zou, X.; Jiang, J.; Qin, K.; Zhang, Y.; Yang, W.; Li, X. Progress in the principle and application of zircon trace element. *Acta Petrol. Sin.* **2021**, *37*, 985–999. (In Chinese with English abstract) [[CrossRef](#)]
21. Anders, E.; Grevesse, N. Abundances of the elements: Meteoritic and solar. *Geochim. Cosmochim. Acta* **1989**, *53*, 197–214. [[CrossRef](#)]
22. Xu, X.S.; O'Reilly, S.Y.; Griffin, W.L.; Wang, X.L.; Pearson, N.J.; He, Z.Y. The crust of Cathaysia: Age, assembly and reworking of two terranes. *Precambrian Res.* **2007**, *158*, 51–78. [[CrossRef](#)]
23. Middlemost, E.A.K. Naming materials in the magma/igneous rock system. *Earth-Sci. Rev.* **1994**, *37*, 215–224. [[CrossRef](#)]
24. McDonough, W.F.; Sun, S.-S. The composition of the Earth. *Chem. Geol.* **1995**, *120*, 223–253. [[CrossRef](#)]
25. Coleman, D.S.; Gray, W.; Glazner, A.F. Rethinking the emplacement and evolution of zoned plutons: Geochronologic evidence for incremental assembly of the Tuolumne intrusive suite, California. *Geology* **2004**, *32*, 433–436. [[CrossRef](#)]
26. Ma, C.Q.; Li, Y.Q. Incremental growth of granitoid plutons and highly crystalline magmatic differentiation. *Acta Petrol. Sin.* **2017**, *33*, 1479–1488. (In Chinese with English abstract)
27. Simon, J.I.; Renne, P.R.; Mundil, R. Implications of pre-eruptive magmatic histories of zircons for U–Pb geochronology of silicic extrusions. *Earth Planet. Sci. Lett.* **2008**, *266*, 182–194. [[CrossRef](#)]
28. Hoskin, P.W.O.; Schaltegger, U. The Composition of Zircon and Igneous and Metamorphic Petrogenesis. *Rev. Mineral. Geochem.* **2003**, *53*, 27–62. [[CrossRef](#)]
29. Scaillet, B.; Holtz, F.; Pichavant, M. Experimental constraints on the formation of silicic magmas. *Elements* **2016**, *12*, 109–114. [[CrossRef](#)]
30. Medlin, C.; Jowitt, S.; Cas, R.; Smithies, R.; Kirkland, C.; Maas, R.; Raveggi, M.; Howard, H.; Wingate, M. Petrogenesis of the A-type, Mesoproterozoic intra-caldera rheomorphic Kathleen ignimbrite and comagmatic Rowland suite intrusions, West Musgrave Province, Central Australia: Products of extreme fractional crystallization in a failed rift setting. *J. Petrol.* **2015**, *56*, 493–525. [[CrossRef](#)]
31. Ustunisik, G.; Kilinc, A. The role of fractional crystallization, magma recharge, and magma mixing in the differentiation of the Small Hasandag volcano, Central Anatolia, Turkey. *Lithos* **2011**, *125*, 984–993. [[CrossRef](#)]
32. Humphreys, M.C.; Blundy, J.D.; Sparks, R.S.J. Magma evolution and open-system processes at Shiveluch Volcano: Insights from phenocryst zoning. *J. Petrol.* **2006**, *47*, 2303–2334. [[CrossRef](#)]
33. Tepley, F.J.; Davidson, J.P.; Tilling, R.L.; Arth, J.G. Magma mixing, recharge and eruption histories recorded in plagioclase phenocrysts from El Chichon Volcano, Mexico. *J. Petrol.* **2000**, *41*, 1397–1411. [[CrossRef](#)]
34. Bachmann, O.; Bergantz, G.W. On the origin of crystal-poor rhyolites: Extracted from batholithic crystal mushes. *J. Petrol.* **2004**, *45*, 1565–1582. [[CrossRef](#)]
35. Deering, C.D.; Bachmann, O.; Vogel, T.A. The Ammonia Tanks Tuff: Erupting a melt rich rhyolite cap and its remobilized crystal cumulate. *Earth Planet. Sci. Lett.* **2011**, *310*, 518–525. [[CrossRef](#)]
36. Guo, F.; Fan, W.; Li, C.; Zhao, L.; Li, H.; Yang, J. Multi-stage crust–mantle interaction in SE China: Temporal, thermal and compositional constraints from the Mesozoic felsic volcanic rocks in eastern Guangdong-Fujian provinces. *Lithos* **2012**, *150*, 62–84. [[CrossRef](#)]
37. He, Z.-Y.; Xu, X.-S. Petrogenesis of the Late Yanshanian mantle-derived intrusions in southeastern China: Response to the geodynamics of paleo-Pacific plate subduction. *Chem. Geol.* **2012**, *328*, 208–221. [[CrossRef](#)]
38. Jackson, M.D.; Blundy, J.; Sparks, R.S.J. Chemical differentiation, cold storage and remobilization of magma in the Earth's crust. *Nature* **2018**, *564*, 405–409. [[CrossRef](#)] [[PubMed](#)]
39. Annen, C.; Blundy, J.D.; Sparks, R.S.J. The genesis of intermediate and silicic magmas in deep crustal hot zones. *J. Petrol.* **2006**, *47*, 505–539. [[CrossRef](#)]
40. Gualda, G.A.; Ghiorsso, M.S. Low-pressure origin of high-silica rhyolites and granites. *J. Geol.* **2013**, *121*, 537–545. [[CrossRef](#)]
41. Ferry, J.M.; Watson, E.B. New thermodynamic models and revised calibrations for the Ti-in-zircon and Zr-in-rutile thermometers. *Contrib. Mineral. Petrol.* **2007**, *154*, 429–437. [[CrossRef](#)]

Disclaimer/Publisher's Note: The statements, opinions and data contained in all publications are solely those of the individual author(s) and contributor(s) and not of MDPI and/or the editor(s). MDPI and/or the editor(s) disclaim responsibility for any injury to people or property resulting from any ideas, methods, instructions or products referred to in the content.